NEUROSCIENCE

Daily changes in light influence mood via inhibitory networks within the thalamic perihabenular nucleus

Tenley Weil[1]†, K. M. Daly[1,2]†, Hector Yarur Castillo[3]†, Michael B. Thomsen[1], Huikun Wang[3], Maria E. Mercau[4], Samer Hattar[1]*, Hugo Tejeda[3]*, Diego C. Fernandez[1]*

Exposure to irregular lighting schedules leads to deficits in affective behaviors. The retino-recipient perihabenular nucleus (PHb) of the dorsal thalamus has been shown to mediate these effects in mice. However, the mechanisms of how light information is processed within the PHb remains unknown. Here, we show that the PHb contains a distinct cluster of GABAergic neurons that receive direct retinal input. These neurons are part of a larger inhibitory network composed of the thalamic reticular nucleus and zona incerta, known to modulate thalamocortical communication. In addition, PHb^{GABA} neurons locally modulate excitatory-relay neurons, which project to limbic centers. Chronic exposure to irregular light-dark cycles alters photo-responsiveness and synaptic output of PHb^{GABA} neurons, disrupting daily oscillations of genes associated with inhibitory and excitatory PHb signaling. Consequently, selective and chronic PHb^{GABA} manipulation results in mood alterations that mimic those caused by irregular light exposure. Together, light-mediated disruption of PHb inhibitory networks underlies mood deficits.

INTRODUCTION

Exposure to irregular light schedules, such as those experienced by shift workers, has become more prevalent in modern society (*1*). When sustained over time, these irregular light conditions can result in deleterious effects on human health, including circadian and sleep disturbances, cognitive deficits, and mood disorders (*2*, *3*). In mammals, ambient light is processed in the retina and routed to brain targets through projection neurons, termed retinal ganglion cells (RGCs). Among RGC subtypes, intrinsically photosensitive melanopsin (*Opn4*)–expressing RGCs (ipRGCs) transmit photic signals that influence innate functions, such as the synchronization of endogenous circadian rhythms to light-dark cycles (*4*–*6*). Studies using animal models, as well as data collected from human subjects, have further implicated ipRGC signaling in modulating metabolic functions, cognition, and affective behavior (*7*–*10*). We have recently delineated an ipRGC brain circuit that drives the deleterious effects of irregular light on mood-related behaviors in mice (*11*). This circuit directs environmental light information to the perihabenular nucleus (PHb) of the dorsal thalamus, which projects to limbic areas including the ventromedial prefrontal cortex (vmPFC), dorsomedial striatum (CPu), and nucleus accumbens (NAc). Manipulation of PHb projections to these limbic targets revealed that the PHb is both necessary and sufficient for mediating the effects of light on mood in mice (*11*, *12*). Although the role of PHb neurons in relaying photic information to limbic areas has been explored, the thalamic circuits and cellular mechanisms that encode and process light information remain unknown.

The mammalian thalamus plays a crucial role in transmitting sensory information to distinct cortical areas (*13*, *14*). Thalamic nuclei are primarily composed of excitatory (glutamatergic) relay neurons (*15*). Unlike the majority of the dorsal thalamus in mice, the retino-recipient dorsal lateral geniculate nucleus (dLGN) contains a subset of inhibitory (GABAergic) interneurons that spatially and temporally synchronize local networks (*15*–*17*). In addition, thalamic nuclei receive inhibitory inputs from areas of the thalamic reticular nucleus (TRN) and an extra-thalamic system composed of forebrain and midbrain nuclei that are thought to modulate and grade output signals, enabling proper thalamocortical functions (*18*). Thalamic targets of RGCs include the dLGN, responsible for image-forming visual functions, as well as nuclei, which govern innate and mood-related behaviors, including the PHb and nuclei of the posterior thalamus (*11*, *19*, *20*). Despite substantial retinal innervation to these thalamic areas, there is a critical gap in our understanding of how light is processed outside image-forming visual networks. In this regard, the ipRGC-PHb circuit represents a unique system to explore the thalamic processing of photic information to influence innate and mood-related behaviors.

Here, we investigated the PHb circuits that process photic signals under regular and irregular light-dark schedules. We found that GABAergic neurons in the dorsal thalamus are clustered in visual centers and form a retino-recipient circuit embedded within the PHb. PHb^{GABA} neurons have local and long-range projections that constitute a larger circuitry of thalamic and subthalamic GABAergic neurons, revealing that the PHb is part of a network that extends beyond the previously described limbic targets (*11*). These long-range inhibitory connections differentiate the PHb from the dLGN, which only contains local inhibitory networks (*21*). PHb^{GABA} neurons are particularly reactive to chronic exposure to irregular light-dark cycles, resulting in alterations in the daily changes in gene expression observed in this nucleus. Disrupting the daily pattern of activity of PHb^{GABA} neurons is sufficient to cause deficits in mood-related behaviors. Together, these results reveal that daily changes in retino-recipient inhibitory networks in the PHb are critical for processing photic input to thalamic circuits that control mood-related behavior in mice.

[1]Section on Light and Circadian Rhythms (SLCR), National Institute of Mental Health, National Institutes of Health, Bethesda, MD 20892, USA. [2]Department of Biology, Johns Hopkins University, 3400 N. Charles Street, Baltimore, MD 21218, USA. [3]Unit on Neuromodulation and Synaptic Integration, National Institute of Mental Health, National Institutes of Health, Bethesda, MD 20892, USA. [4]Department of Immunobiology, School of Medicine, Yale University, New Haven, CT 06520, USA.
*Corresponding author. Email: diego.fernandez@nih.gov (D.C.F.); hugo.tejeda@nih.gov (H.T.); samer.hattar@nih.gov (S.H.)
†These authors contributed equally to this work.

RESULTS

The PHb contains retino-recipient GABAergic neurons

The cellular architecture of thalamic PHb circuits was investigated in adult wild-type (WT) mice. Excitatory-relay neurons were identified by *Slc17a6* (*Vglut2*) expression, which is found in excitatory neurons in subcortical structures, including the thalamus (*22*). In situ hybridization assays revealed that excitatory-relay neurons are homogeneously distributed throughout the dorsal thalamus and represent ~74% of neurons that constitute the PHb (Fig. 1, A to C). We further identified a dense population of GABAergic neurons in the PHb (Fig. 1, B and C, and fig. S1A), as revealed by the coexpression of the vesicular GABA transporter (*Vgat*) and glutamate decarboxylase 1 and 2 (*Gad1* and *Gad2*, respectively; Fig. 1D). PHb^{GABA} neurons did not express markers of interneurons previously described for thalamic nuclei (*23*–*25*), including parvalbumin and somatostatin (fig. S1B). Electrophysiological characterization of PHb^{GABA} neurons identified three functional subpopulations, defined as fast spiking, quasi–fast spiking cells, and cells that readily entered depolarization block with depolarizing current pulses (fig. S1, C and D).

To properly determine the topographic distribution of GABAergic neurons in the dorsal thalamus, we used a mouse line expressing the reporter gene *mCherry* directed by the endogenous *Gad2* promoter ($GAD2^{mCherry}$ mice). $GAD2^{+}$ neurons form a distinct cluster located within the PHb, distributed most densely in its caudal region (Fig. 1, E to G). In addition, GABAergic neurons were observed in the dLGN (fig. S1D), as previously reported (*26*); $GAD2^{+}$ cells were either absent or sparsely distributed in neighboring nuclei of the dorsal thalamus (Fig. 1E and fig. S1E). These results were further confirmed using in situ hybridization for GABAergic markers in WT mice (fig. S1, F and G).

Retino-recipient PHb^{GABA} neurons locally connect to excitatory-relay neurons

The PHb is densely innervated by retinal fibers, especially in its caudal region (*11*), where GABAergic neurons are most abundant. Here, we mapped retinal innervation in $GAD2^{mCherry}$ mice using intravitreal injections of the tracer cholera toxin b-subunit (CTb). We observed that the pattern of retinal innervation to the PHb closely overlaps with the distribution of $GAD2^{+}$ cells (Fig. 1, E to G), suggesting a direct modulation of interneuron function by photic signals. To test this possibility, we first used a monosynaptic rabies virus tracing strategy to determine whether RGCs make direct connections with GABAergic cells in the PHb. $GAD2^{Cre}$ mice were injected in the PHb with a *Cre*-dependent adeno-associated virus (AAV)/TVA–oG–green fluorescent protein (GFP), and 4 weeks later, mice were injected in the PHb with a G-deleted rabies-mCherry virus (Fig. 1H and fig. S2A). We observed retrogradely labeled RGCs throughout the retina (fig. S2B), most of them (82%) were immunopositive for melanopsin, belonging to M1 (60%) and M4 (40%) ipRGC subtypes (Fig. 1I and fig. S2C). Retinal input to PHb^{GABA} neurons was further evaluated using an optogenetic strategy. Specifically, channelrhodopsin-2 (ChR2) was expressed in retinal terminals [intravitreal injection of an AAV2/ChR2–enhanced yellow fluorescent protein (EYFP) in the eye], and whole-cell electrophysiological recordings were obtained from PHb neurons in $GAD2^{mCherry}$ mice (Fig. 1J). Activation of ChR2-expressing retinal terminals by flashes of blue light evoked excitatory postsynaptic currents in a subset of GABAergic neurons in the PHb (Fig. 1, K and L), as well as excitatory-relay neurons (fig. S2D). Together, these results confirm that ipRGCs have monosynaptic contacts with GABAergic cells within the PHb, in addition to excitatory-relay neurons, expanding on previous observations (*11*, *12*).

To determine whether retino-recipient GABAergic cells modulate local PHb circuits, we traced the projections of these neurons by injecting a *Cre*-dependent AAV expressing fluorophores that label the cellular projections (tdTomato) as well as synaptic terminals (GFP) into the PHb of $GAD2^{Cre}$ mice (Fig. 2A). First, we observed that PHb^{GABA} neurons have dense local connections within the caudal PHb and project to neighboring areas of the dorsal thalamus (Fig. 2, B and C). GABAergic neurons, which are located primarily in the caudal PHb, also show projections that spread to the rostral areas of the nucleus (Fig. 2D and fig. S2E), suggesting that these GABAergic cells may modulate functional responses of both local and (rostrally) distant excitatory-relay PHb neurons. To test this, $GAD2^{Cre}$ mice were injected in the PHb with a *Cre*-dependent AAV expressing ChR2-eYFP (fig. S2F). Optogenetic stimulation of ChR2-expressing GABAergic PHb neurons evoked inhibitory postsynaptic currents (oIPSCs) in excitatory-relay neurons distributed throughout the rostro-caudal PHb (fig. S2, G and H), consistent with the widespread projections of PHb^{GABA} cells. Activation of PHb^{GABA} neurons inhibits evoked spiking in excitatory-relay neurons, and this effect is blocked by the $GABA_A$ receptor antagonist picrotoxin (fig. S2I). In addition, oIPSCs were abolished by blocking action potential propagation with tetrodotoxin (TTX) and reinstated after the addition of the potassium channel blocker 4-AP (fig. S2J), demonstrating that excitatory-relay neurons receive functional monosynaptic inputs from PHb^{GABA} neurons. Combined, these results demonstrate that the PHb contains a distinct cluster of retino-recipient GABAergic neurons, which make functional monosynaptic connections onto excitatory-relay neurons throughout the PHb.

The PHb is part of a larger inhibitory thalamic and subthalamic network

Our tracing analysis suggested that PHb^{GABA} neurons, in addition to their local connections, might extend projections outside the PHb region. It was recently proposed that a discrete pathway of PHb projections to the NAc contains GABAergic fibers (*12*). By investigating the projection pattern of PHb^{GABA} neurons in $GAD2^{Cre}$ mice injected with the *Cre*-dependent AAV expressing tdT-2A-SynGFP (Fig. 2A), we observed sparse or even complete absence of innervation from PHb^{GABA} neurons in the NAc, vmPFC, and CPu (Fig. 2E), target areas of excitatory-relay PHb neurons (*11*). The projections of PHb^{GABA} neurons into the NAc or vmPFC were further explored using retrograde AAVs (retroAAVs) injected in the NAc or vmPFC (fig. S3, A and E). We found that GABAergic neurons represent a minor fraction of total NAc-projecting PHb neurons compared with excitatory-relay cells (fig. S3, A to D). In addition, we found that while the vmPFC receives substantial input from excitatory-relay PHb neurons, GABAergic innervation to this region is virtually absent (fig. S3, E and F).

A comprehensive analysis of the GABAergic projections revealed that PHb^{GABA} neurons have a substantial widespread pattern of thalamic connectivity that goes beyond local PHb circuits (Fig. 2F). PHb^{GABA} neurons extensively innervate the caudal region of the contralateral PHb, the dorsal portion of the TRN, and the subthalamic zona incerta (Zi; Fig. 2, F to J). The synaptophysin-fused GFP puncta observed in these areas suggest the presence of synaptic

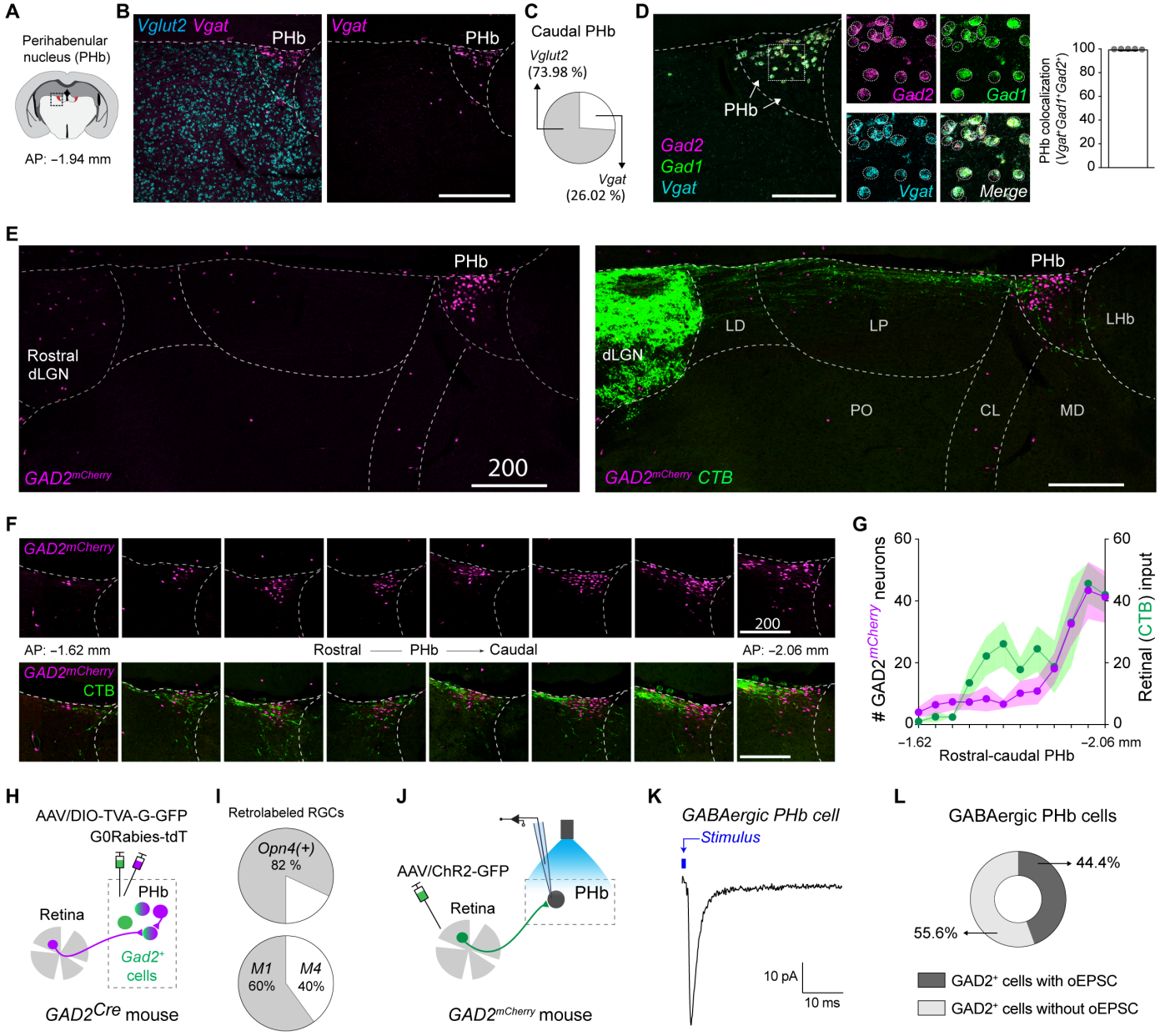

Fig. 1. Cellular arrangement of the retino-recipient PHb. (**A**) Schematic of a coronal brain section highlighting the PHb. (**B** and **C**) Representative in situ labeling of excitatory-relay (*Vglut2*$^+$) and inhibitory (*Vgat*$^+$) PHb neurons are shown (B). Percentages of PHb *Vglut2*$^+$ and *Vgat*$^+$ neurons (C). Data are means ± SEM ($n = 5$ mice). (**D**) Representative images showing the coexpression of *Vgat*, *Gad1*, and *Gad2* in PHb neurons. Data are means ± SEM ($n = 5$ mice). (**E**) Representative images of *GAD2*^{mCherry} cells and retinal fiber (CTB) distribution in the dorsal thalamus. (**F** and **G**) Rostro-caudal distribution of *GAD2*$^+$ neurons and retinal fibers in the PHb (F). Rostral to caudal PHb sections were defined by anteroposterior coordinates (distance to bregma). The number of *GAD2*$^+$ neurons correlates with retinal inputs to the PHb (G). Retinal input is expressed as the percentage of total PHb area covered by CTB$^+$ retinal fibers. Data are means ± SEM ($n = 4$ mice). Spearman's correlation $r = 0.7902$, $P = 0.0033$. (**H** and **I**) Schematic of the monosynaptic rabies virus strategy (H). A total of 82% of the retrolabeled RGCs were melanopsin immunopositive (I); 60% of retrolabeled cells corresponded to the M1 ipRGC subtype, and 40% to the M4 subtype. (**J** to **L**) Optogenetic evidence for functional connections between retinal terminals and PHb neurons. Current response to light stimulation in a representative PHb^{GABA} neuron is shown (K). A fraction of total PHb^{GABA} neurons ($n = 9$ cells) showed ChR2-induced responses (L). LHb, lateral habenula; LD, lateral dorsal nucleus; LP, lateral posterior nucleus; PO, posterior complex; CL, central lateral nucleus; MD, mediodorsal nucleus. Scale bars, 100 mm (D) and 200 mm (B, E, and F). See also figs. S1 and S2.

contacts with target neurons (Fig. 2, G to I). Tracing tools to retrogradely label *GAD2*$^+$ cells projecting to the PHb, and a monosynaptic rabies virus strategy have further revealed that PHb^{GABA} neurons are embedded in an inhibitory network that bidirectionally connects the dorsal thalamus with the TRN and Zi (fig. S3, G to L), areas known to send inhibitory input to thalamic territories (*18*). These results revealed that PHb^{GABA} neurons, in addition to having local connections, are part of a larger inhibitory thalamic and subthalamic network (Fig. 2K), a unique aspect of the PHb compared with other thalamic nuclei.

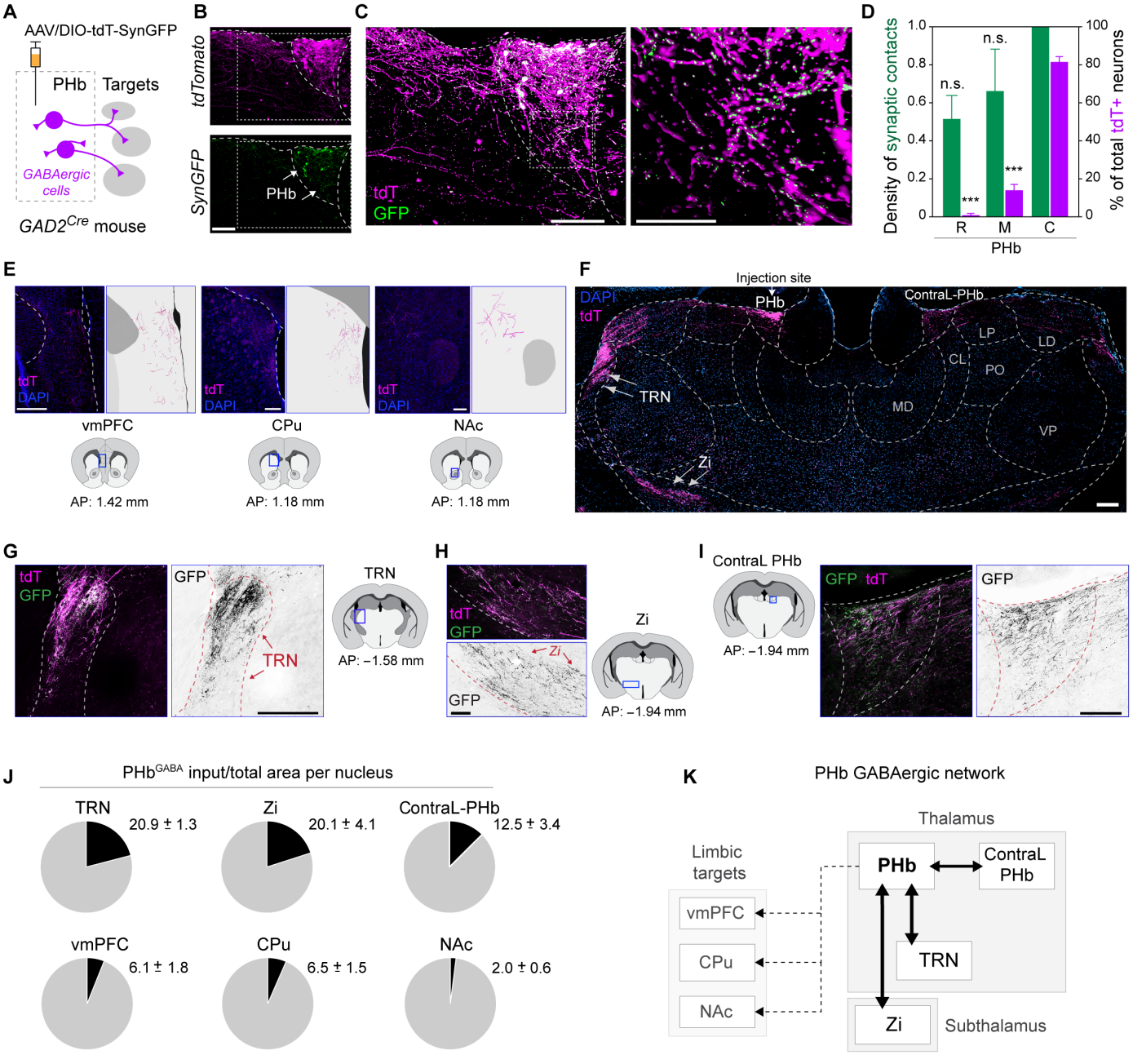

Fig. 2. Connectivity of PHb^{GABA} neurons. (**A**) *Cre*-dependent AAVs expressing cytoplasmic tdTomato (tdT) and (presynaptic) synaptophysin-fused eGFP were injected into the PHb in *GAD2*^{Cre} mice. (**B** to **D**) GABAergic projections were found throughout the PHb and neighboring areas (B and C). Rostro-caudal distribution of synaptic input (green) and somas (magenta) of PHb^{GABA} neurons were quantified in (D). Results are expressed as density of SynGFP^{+} puncta relative to total puncta observed in the caudal PHb. In addition, the distribution of GABA^{tdT+} cells in the PHb is shown. Rostral (R), middle (M), and caudal (C) PHb regions were determined on the basis of brain coordinates (see Materials and Methods). Data are means ± SEM ($n = 4$ mice). ***$P < 0.001$, compared with caudal PHb, one-way analysis of variance test. n.s., not significant. (**E**) Sparse PHb^{GABA} (tdT^{+}) fibers were observed in the vmPFC, CPu, and NAc. Representative images and reconstructions of PHb^{GABA} projections are shown. (**F** to **I**) Dense PHb^{GABA} projections were observed in the contralateral PHb, ipsilateral TRN, and Zi (F; arrows indicate ipsilateral projections). Representative images of PHb^{GABA} fibers (tdT^{+}) and synaptic contacts (GFP^{+}) with target cells located in the TRN (G), Zi (H), and contralateral PHb (I). (**J**) The area of PHb^{GABA} innervation relative to total nuclei area was quantified. Data are means ± SEM ($n = 5$ mice). (**K**) Schematic describing the inhibitory thalamic network containing the PHb^{GABA} neurons. Solid lines indicate bidirectional connections, whereas dotted lines represent projections from PHb^{GABA} cells. VP, ventral posterior complex. Scale bars, 50 mm (C inset), 100 mm (B and C), and 200 mm (E to I). See also figs. S2 and S3.

Irregular light exposure disrupts daily expression of genes that govern neurotransmission balance of the PHb

We previously showed that under irregular light-dark schedules, photic signals driven by excitatory-relay PHb neurons to limbic targets alter mood-related behaviors in mice (*11*). Our current results revealed that the PHb also contains retino-recipient GABAergic neurons that locally modulate excitatory-relay neurons. Therefore, we investigated the extent to which abnormal light cues cause alterations within PHb circuits. To do this, we used RNA sequencing (RNA-seq) to comprehensively examine tissue-wide transcriptional changes occurring within the PHb. Mice were housed under regular (T24 cycle) or irregular (T7 cycle, alternating periods of 3.5 hours of light and darkness for 2 weeks) light-dark schedules. PHb samples were collected either during the active [circadian time (CT)14] or inactive (CT2) phase according to mouse activity (Fig. 3A and fig. S4, A and B). All biological replicates showed a strong enrichment for thalamic marker genes (Fig. 3B), confirming the accuracy of the tissue dissections. Analysis of transcriptional changes between the active and inactive phases of mice housed under the T24 cycle revealed genes that were differentially expressed, including the clock gene *Per2*, GABA receptor A subunit *Gabrr2*, and integral membrane components (*Cldn5* and *Gja5*; Fig. 3C and fig. S4C). Functional annotation of differentially regulated genes indicated that up-regulated genes at CT14 play a critical role in circadian and biological rhythms, and transcriptional regulation, whereas genes that are up-regulated during the inactive phase are associated with cytoarchitectural reorganization (Fig. 3D). To gain a broad understanding of normal phasic changes in gene expression across the day/night cycles, we performed gene set enrichment analysis (GSEA) (*27*). We found that genes associated with GABAergic synaptic transmission were enriched during the active phase of mice (CT14), whereas genes involved in cellular respiration were enriched during the inactive phase (CT2; fig. S4D).

We next examined whether the daily transcriptional changes in PHb neurons are affected by the chronic exposure to an irregular light schedule (T7 cycle; Fig. 3A). Notably, we found that exposure of mice to an irregular light-dark schedule disrupted the phasic nature of gene expression observed under regular lighting conditions (Fig. 3E). Genes displaying robust phasic changes under regular light conditions were substantially altered after irregular light exposure (Fig. 3E). GSEA comparing samples collected at CT14 from mice housed under the T7 cycle and the T24 cycle showed that genes involved in membrane depolarization and regulation of glutamate secretion were enriched after irregular light exposure (fig. S4D). Collectively, these results suggest that the chronic and abnormal activation of photo-responsive circuits induced by irregular light schedules causes widespread alterations in the daily oscillations of gene expression and neurotransmission of PHb neurons.

To further understand how irregular light schedules affect neurotransmission in the PHb, we examined the expression of genes associated with synaptic transmission under normal and irregular light schedules. Under the T24 cycle, most genes associated with GABAergic signaling displayed phasic changes, including genes involved in GABA metabolism (e.g., *Gad1*, *Gad2*, and *Abat*), transporters (e.g., *Slc6a1* and *Slc6a11*), and receptors (e.g., *Gabrq*, *Gabra1*, and *Gabrg2–3*; fig. S4E). Phasic changes in gene expression levels under regular conditions were also observed in genes associated with glutamatergic signaling (fig. S4F). Exposure to irregular light-dark cycles, however, resulted in a weakened phasic expression of nearly all GABAergic and glutamatergic genes (fig. S4, E and F). Alterations in the expression pattern of GABAergic and glutamatergic genes were validated using in situ hybridization labeling. First, we confirmed that, under regular lighting conditions, the expression levels of GABAergic (*Gabra5* and *Gabra2*) and glutamatergic (*Grin2a* and *Camk2a*) genes in the PHb were significantly different at different phases of mice activity (T24 cycle; Fig. 3F and fig. S5). We further established that the observed daily oscillations in gene expression were abolished after irregular light exposure (T7 cycle; Fig. 3F and fig. S5). Together, our transcriptional analyses revealed that abnormal light exposure disrupts the daily oscillations in genetic programs within the PHb that govern neurotransmission homeostasis in these circuits.

Exposure to irregular light schedules disrupts local inhibitory control within the PHb

Irregular light exposure causes extensive changes in daily gene expression at a tissue-wide level in the PHb. To investigate the molecular mechanisms underlying the light-mediated changes in the PHb, we determined the photo-responsiveness of PHb neurons in $GAD2^{mCherry}$ mice housed under either T24 or T7 cycles for 2 weeks (Fig. 4A). Under regular lighting conditions, both GABAergic and excitatory-relay neurons show robust light-mediated induction of the immediate-early gene *Fos* (also known as c-Fos) throughout the PHb (Fig. 4, B to E, and fig. S6A). We observed a significant increase in the number of $c\text{-}Fos^{+}$ GABAergic neurons in mice exposed to T7 cycles compared with the T24 cycle (Fig. 4, D and E), suggesting that PHb^{GABA} neurons are sensitized because of the irregular light stimulation.

Next, we investigated whether the enhanced photo-responsiveness of PHb^{GABA} neurons was associated with changes in their intrinsic excitability. Whole-cell recordings from PHb^{GABA} neurons in ex vivo brain slices were obtained from $GAD2^{mCherry}$ mice exposed to T24 or T7 light cycles. We found that an increased fraction of PHb^{GABA} neurons were spontaneously active in mice exposed to the T7 cycle, compared with the T24 cycle, showing an increase in basal firing rates (Fig. 4F). We then determined whether the increased spontaneous activity of PHb^{GABA} neurons affects excitatory-relay neurons. We observed that the T7 cycle caused a significant increase in the frequency of spontaneous IPSCs (sIPSCs) in excitatory-relay PHb neurons relative to controls, with no changes in sIPSC amplitude (Fig. 4G). In addition, no differences in miniature IPSCs (mIPSCs) frequency or amplitude were observed between groups (fig. S6, B and C). Together, these results indicate that increased spontaneous firing rate of PHb^{GABA} neurons drive increased inhibitory synaptic transmission onto excitatory-relay neurons. To determine the efficacy of synaptic transmission between local GABAergic outputs to excitatory-relay PHb neurons, we recorded optogenetically evoked IPSCs (oIPSCs) in excitatory-relay PHb neurons in $GAD2^{Cre}$ mice expressing ChR2-eYFP and housed under T24 or T7 light cycles (fig. S6D). We found that PHb^{GABA} evoked oIPSCs in excitatory-relay neurons were enhanced in T7 cycle–housed mice, relative to control mice (fig. S6, E and F). No differences in the coefficient of variation, paired pulse ratio, or depression of oIPSCs during trains of differing frequencies were observed, consistent with no change in presynaptic probability of release or short-term plasticity at these synapses (fig. S6, G to N). Together, these results revealed that the chronic exposure to irregular light-dark cycles enhanced the photo-responsiveness and excitability of PHb^{GABA} neurons, strengthened GABAergic connections, and increased action potential–dependent GABA release onto excitatory-relay PHb neurons.

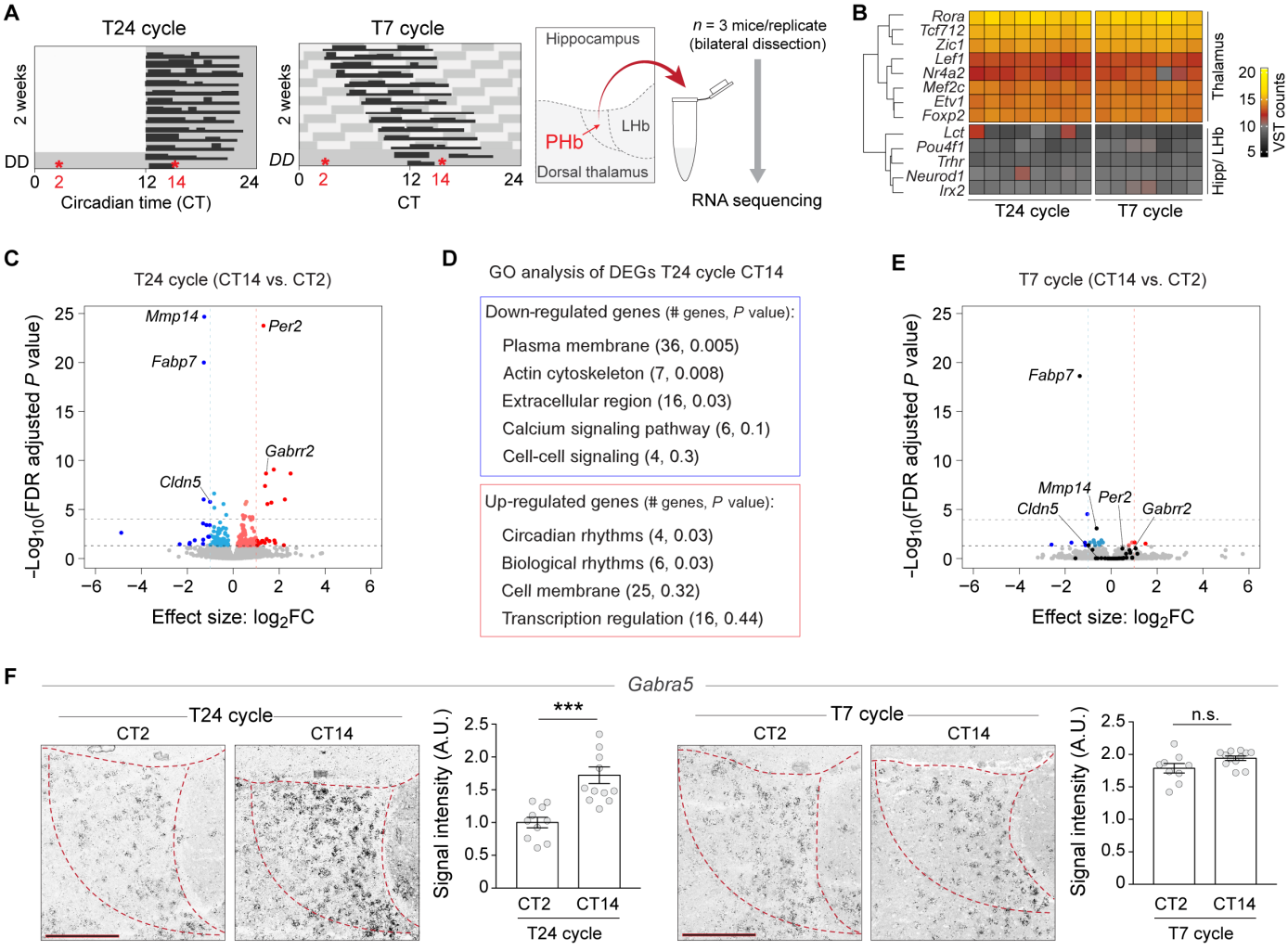

Fig. 3. Irregular light exposure disrupts daily oscillations of gene expression in the PHb. (**A**) Mice were housed under the T24 or T7 cycles for 2 weeks and 1 day under constant darkness (DD). PHb samples were collected at CT2 or CT14. Samples (bilateral dissection) collected from three mice were combined. Four replicates were analyzed per condition. (**B**) Heatmap of normalized gene expression (variance stabilizing $\log_2$-transformed counts) across samples for reported transcription factors enriched in the thalamus (*Rora*, *Tcf7l2*, *Zic1*, *Lef1*, *Nr4a2*, *Mef2c*, *Etv1*, and *Foxp2*), habenular complex (*Pou4f1*, *Neurod1*, and *Irx2*), and marker genes specific to granule cells in the hippocampus (*Lct* and *Trhr*). (**C**) Volcano plot showing the significant differentially expressed genes between active (CT14) and inactive (CT2) periods of mouse activity under the T24 cycle (FDR < 0.05 and $|\log_2 FC| > 1$). Red and blue points represent significantly up-regulated and down-regulated genes, respectively, at CT14. (**D**) Functional annotation of DEGs. (**E**) Volcano plot of differentially expressed genes in mice housed under the irregular T7 cycle. Black points represent DEGs found to be significantly and differentially expressed under the T24 cycle. Note that *Fabp7*, the fatty acid binding protein 7 gene expressed by astrocytes, was the only gene to remain significantly changed after T7 cycle exposure, suggesting that glial cells could perverse rhythmicity. (**F**) Representative images of in situ (RNAscope) labeling of *Gabra5* are shown. Daily changes in gene expression under regular light cycles were abrogated after chronic T7 cycle exposure. Data are means ± SEM. ***$P < 0.001$, two-tailed Student's *t* test. Scale bar, 50 μm (F). A.U., arbitrary unit. See also figs. S4 and S5.

Selective and chronic stimulation of PHb^{GABA} neurons causes mood-related deficits

Our results revealed that PHb^{GABA} neurons are particularly altered under irregular light conditions, suggesting that GABAergic neurons play a central role in modulating local function of PHb circuits. We therefore hypothesized that exclusively disrupting the daily oscillations of PHb^{GABA} neurons might be sufficient to alter local processing of PHb circuits and, ultimately, their output signals. To test this, we used a chemogenetic strategy based on designer receptors exclusively activated by designer drugs (DREADDs) (*28*) to evaluate the transcriptional and behavioral impact of chronic and irregular activation of PHb^{GABA} neurons. *GAD2*^{Cre} mice were bilaterally injected in the PHb with a *Cre*-dependent AAV encoding an excitatory (Gq) receptor or a control AAV/tdTomato (Fig. 5A). Four weeks after injection, mice received the designer ligand clozapine-*N*-oxide (CNO) in their drinking water for 2 weeks to selectively activate neurons expressing the designer receptor (hM3Dq; Fig. 5, A and B, and fig. S7A). Under regular T24 cycles, mice have the highest level of activity and water intake during the night (*11*, *29*), therefore causing chronic and irregular activation of PHb^{GABA} neurons due to CNO intake. No significant changes in locomotor activity were observed during CNO treatment (fig. S7, B to D). We first evaluated the effects of this paradigm on the expression levels of genes associated with GABAergic and glutamatergic signaling. PHb samples

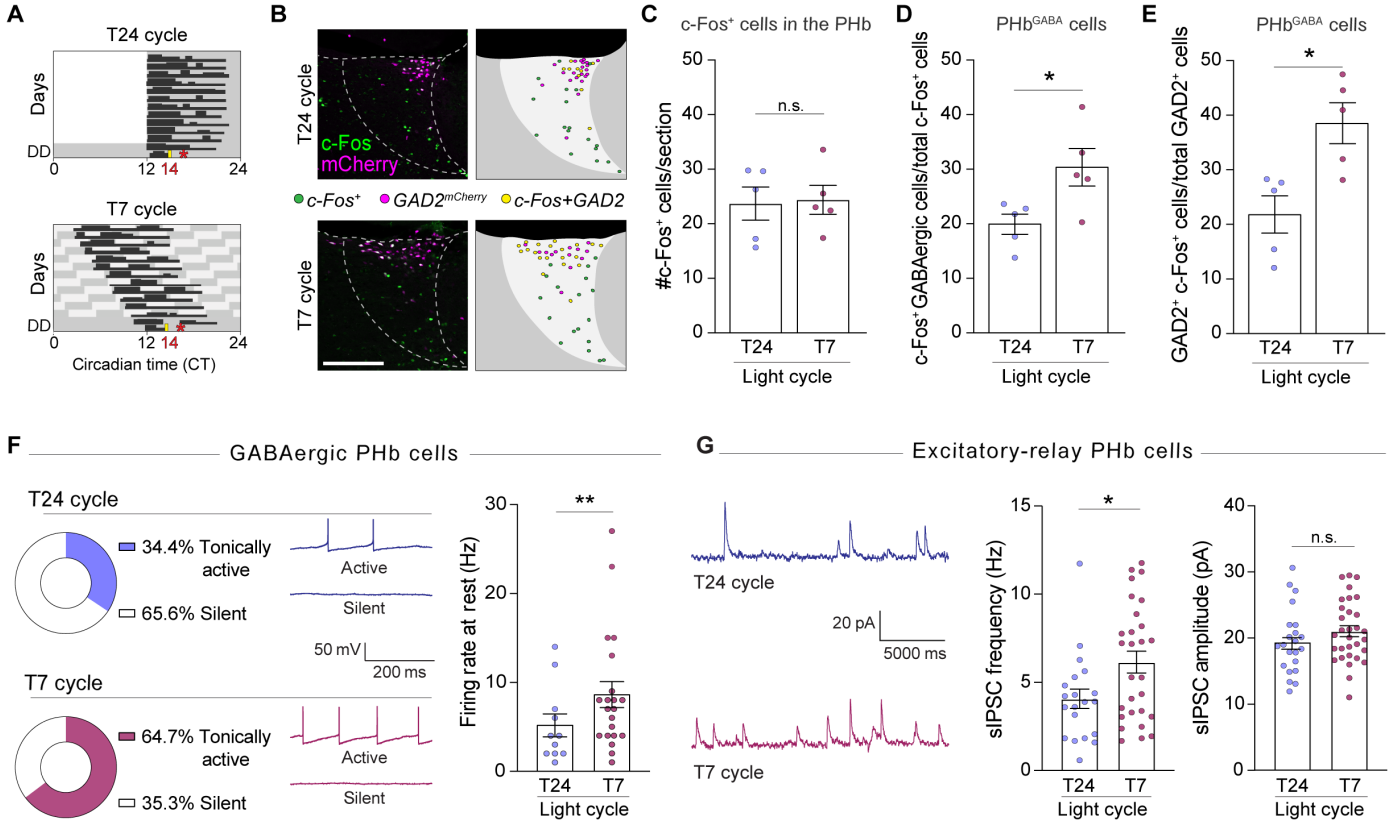

Fig. 4. Irregular light exposure disrupts GABAergic signaling within the PHb. (**A**) Mice were housed under the T24 or T7 cycles for 2 weeks, 1 day in constant darkness (DD), and, lastly, exposed to a light pulse at CT14 (mouse active phase). (**B**) Representative images and reconstructions of light-mediated c-Fos induction (green) in *GAD2*^{mCherry} mice. (**C**) Total number of light-induced c-Fos$^+$ cells observed in the PHb under T24 or T7 light cycles. Data are means ± SEM ($n = 5$ mice), two-tailed Student's *t* test. (**D**) Fraction of total c-Fos$^+$ cells that are GABAergic (*GAD2*$^{mCherry+}$) PHb neurons. Data are means ± SEM ($n = 5$ mice). *$P < 0.05$, two-tailed Student's *t* test. (**E**) Percentage of total *GAD2*^{mCherry} PHb cells that are c-Fos$^+$. Data are means ± SEM ($n = 5$ mice). *$P < 0.05$, two-tailed Student's *t* test. (**F**) Percentage of spontaneously active PHb^{GABA} neurons under the T24 or T7 light cycles. Representative traces of silent and spontaneously active PHb^{GABA} neurons are shown (left). Mean firing rate of spontaneously active PHb^{GABA} neurons (right). Data are means ± SEM ($n = 8$ to 10). **$P < 0.01$, two-tailed Student's *t* test. (**G**) sIPSC frequency and amplitude of excitatory-relay PHb neurons under the T24 or T7 light cycles. Representative traces of sIPSCs from excitatory-relay PHb neurons are shown. Data are means ± SEM ($n = 10$ to 11 mice). *$P < 0.05$, two-tailed Student's *t* test. Scale bar, 100 μm (B). See also fig. S6.

were collected from control and DREADD-expressing mice that were chronically exposed to CNO in the drinking water, and gene expression was quantified using quantitative polymerase chain reaction (qPCR). We found a significant decrease in the expression level of genes involved in GABAergic signaling, including those involved in GABA transporter and metabolism (*Vgat*, *Gad1*, and *Gad2*), and a significant increase in GABAergic receptors (*Gabra2* and *Gabra4*; Fig. 5C). The expression of genes associated with glutamatergic signaling was also altered. Specifically, we observed significantly decreased expression in genes that regulate glutamate metabolism (*Gls2*), an increase in excitatory synapse expression (*C1ql3*, *Camk2b*, and *Slc17a7*), and significant changes in ionotropic (*Gria2* and *Grik1*) and metabotropic (*Grm5*) receptor expression (Fig. 5D). Collectively, these results demonstrate that aberrant activation of PHb^{GABA} neurons promotes the disruption in the PHb transcriptional profile.

Next, we evaluated whether the chronic manipulation of PHb^{GABA} neurons would be sufficient to drive behavioral deficits. Using the same chemogenetic paradigm (Fig. 5A), we found that irregular activation of PHb^{GABA} neurons caused deficits in mood-related behavioral responses. Specifically, mice expressing DREADD receptors in PHb^{GABA} neurons displayed significantly increased immobility time during forced swim (Fig. 5E) and tail suspension (Fig. 5F) tests. Furthermore, we observed deficits in the novelty-suppressed feeding test, as reflected by the significant increased latency to approach and consume food (Fig. 5G and fig. S7, E and F). Together, these results revealed that chronically altering the regular function of inhibitory networks of the PHb, even in mice housed under regular light-dark cycles, is sufficient to cause behavioral manifestations of mood deficits.

DISCUSSION

The PHb has been recently identified and characterized as a thalamic center that regulates mood in mice in response to environmental changes in light (*11*). Previous studies have shown that abnormal photic signals driven by PHb neurons that project to the vmPFC, CPu, and NAc cause deficits in mood-related behaviors (*11*, *12*). Here, we have dissected the thalamic circuits that locally encode and process light information to influence mood. Specifically, we

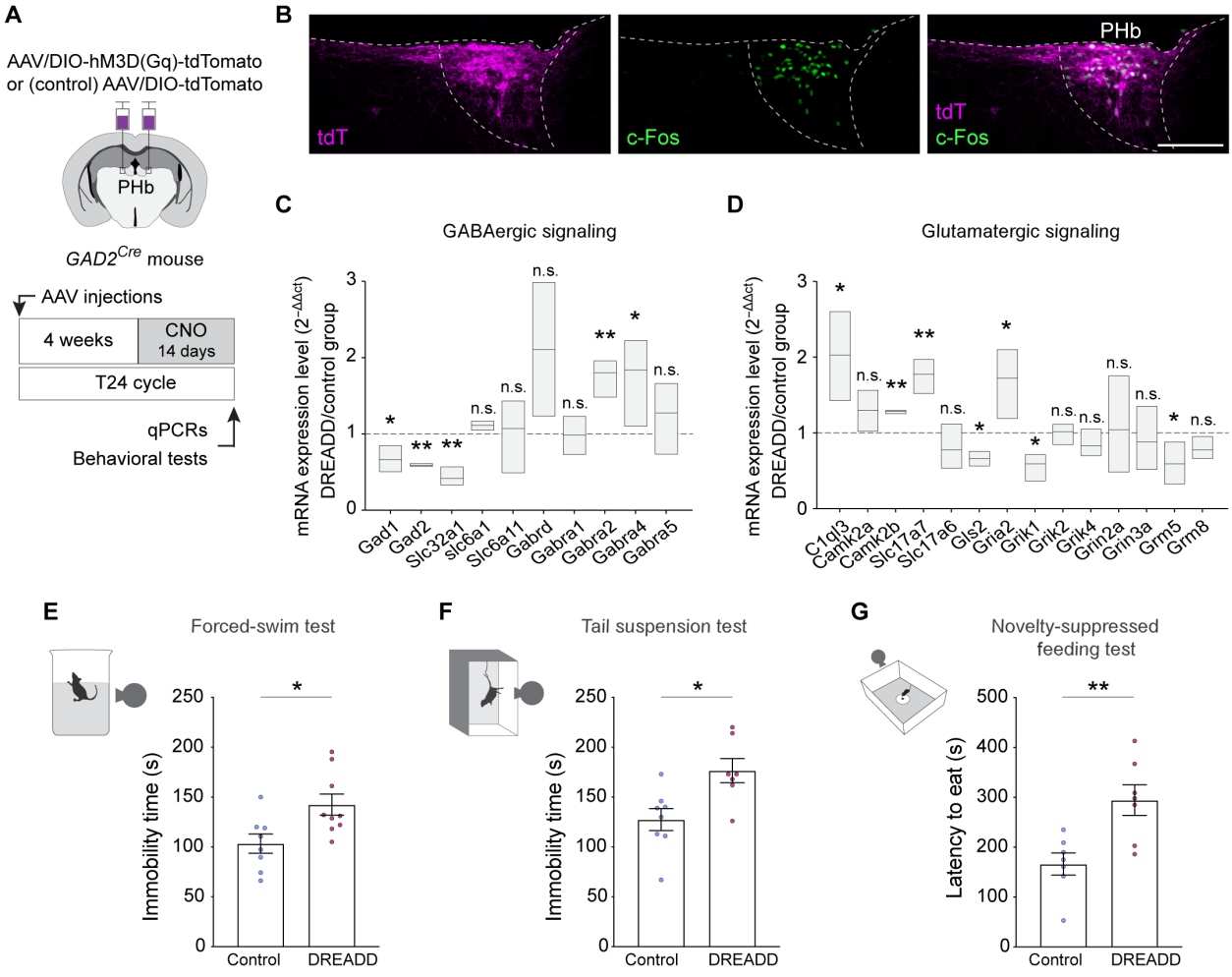

Fig. 5. Chronic manipulation of PHb^{GABA} neurons. (**A**) *Cre*-dependent DREADD-expressing and control AAVs expressing tdTomato were bilaterally injected into the PHb of *GAD2*^{Cre} mice. After 4 weeks, animals were housed under regular T24 cycle with access to CNO in their drinking water for 2 weeks. (**B**) Injection sites were evaluated for tdTomato expression in PHb^{GABA} neurons; c-Fos induction (green) was used to confirm CNO-induced neuronal activation. Representative images are shown. Quantification is shown in fig. S7A. (**C** and **D**) Relative mRNA expression ($2^{-\Delta\Delta ct}$) comparing chronic DREADD activation of PHb^{GABA} neurons to the control group for GABAergic (C) and glutamatergic (D) signaling molecules. Biological replicates ($n = 3$) pooled samples. The statistical analysis compared to the control group (hypothetical value = 1, dotted lines) was performed. *$P < 0.05$, **$P < 0.01$, one sample *t* test. (**E** to **G**) Chronic activation of PHb^{GABA} neurons leads to behavioral manifestations of mood alterations, as shown in the forced-swim (E), tail suspension (F), and novelty-suppressed feeding (G) tests. Data are means ± SEM ($n = 8$ to 9 mice). *$P < 0.05$, **$P < 0.01$, two-tailed Student's *t* test. Scale bar, 100 μm (B). See also fig. S7.

reveal that light detected and routed by ipRGCs directly modulates the function of a retino-recipient inhibitory circuit of the PHb that locally influences excitatory-relay neurons. This inhibitory PHb network is also part of a larger thalamic and subthalamic GABAergic network. Disruption of the GABAergic circuit by selective chemogenetic manipulation of PHb^{GABA} neurons causes severe deficits in mood-related behavior.

GABAergic neurons in the dorsal thalamus form distinct clusters

GABAergic neurons were described in nuclei of the dorsal thalamus of multiple mammalian species (*30*, *31*). However, it was postulated that, with the exception of the visual dLGN, GABAergic neurons were virtually absent in the thalamus of rodents, particularly mice and rats (*32*). Recent studies have reported a wider complexity of ontogenetically and molecularly distinct interneurons present in the mouse thalamus (*25*). Here, we found that PHb^{GABA} neurons, which are defined by the coexpression of *Vgat*, *Gad1*, and *Gad2*, do not express parvalbumin or somatostatin, classic markers of TRN neurons (*23*, *24*), or nNOS, previously shown to delineate a subpopulation of dLGN interneurons (*33*). Functional characterization of PHb^{GABA} cells revealed that a fraction of them display fast-spiking responses, characteristic of *Pvalb*$^{+}$ interneurons, whereas a subpopulation of GABAergic neurons displayed quasi–fast-spiking responses or readily entered depolarization block with minimal current injection. Collectively, these results suggest that PHb^{GABA} neurons constitute a unique cluster of inhibitory interneurons within the thalamus. Future experiments combining functional, morphological, and genetic analyses will properly identify subpopulations of thalamic GABAergic neurons in the PHb. A distinct feature of

GABAergic PHb neurons is that they receive direct retinal innervation from ipRGCs and locally modulate the function of excitatory-relay neurons, similar to previous studies describing retino-thalamic circuits in the dLGN (*13*, *17*). Our results indicate that GABAergic neurons in the dorsal thalamus are clustered within the retino-recipient nuclei, the dLGN, and the PHb (*32*). Therefore, we propose that similar circuit motifs are conserved between retino-recipient areas, suggesting that GABAergic neurons play a major role in modulating the flow of photic signals from the dorsal thalamus to cortical areas.

GABAergic neurons are classically defined as interneurons that temporally and spatially synchronize excitatory neurons within local circuits (*34*). Unlike GABAergic cells in the dLGN (*21*), we found that PHb^{GABA} neurons have both local and long-range projections. This represents a unique aspect of PHb circuitry compared with other nuclei of the dorsal thalamus (*25*, *26*). Long range–projecting GABAergic neurons have been described in other brain circuits. Examples include medium spiny neurons in the striatum, which are the main output projection cells of this brain region (*35*), Purkinje cells in the cerebellum (*36*), and inhibitory interneurons connecting the hippocampus-medial septum (*37*, *38*), which are thought to modulate long-range synchrony between these brain areas (*39*). Our results revealed that long range–projecting PHb^{GABA} neurons form an inhibitory network with the TRN and Zi. It has been postulated that input from TRN and Zi might coordinate gain and acute control of thalamic function to influence thalamocortical signaling (*18*). Further studies will determine the features of the distinct inhibitory input sources to GABAergic and/or excitatory-relay PHb neurons, enabling coordinated thalamic and thalamocortical communication.

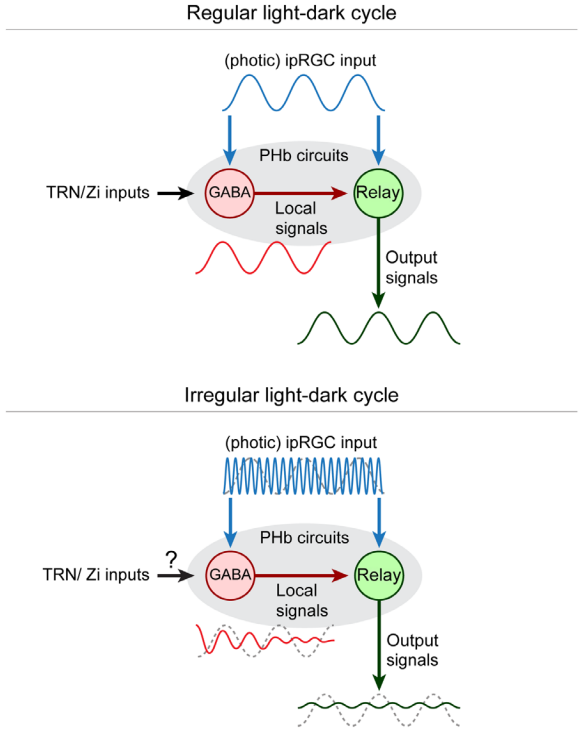

Fig. 6. Model describing excitatory and inhibitory signals within the PHb. Proposed model describing neuronal PHb networks that encode and process light information in mice housed under regular conditions (top) or when lighting conditions become chronically irregular (bottom).

Daily changes occur in excitatory and inhibitory signals of the PHb

PHb neurons display daily changes in the expression of genes that govern the balance of inhibitory and excitatory transmission within these circuits. Both excitatory and inhibitory neurons in the PHb displayed photo-responsiveness, suggesting that daily changes in ambient light may synchronize PHb circuits. We propose that the PHb^{GABA} circuit integrates external and internal signals, through ipRGC and thalamic inputs, respectively, to temporally coordinate the daily oscillations that control the overall function of PHb circuits and output signals (Fig. 6). We found that the chronic exposure to irregular light-dark cycles disrupts the daily gene expression at a tissue-wide level in the PHb. These results are in contrast with the preserved rhythmic function of the SCN observed in mice housed under the T7 cycle (*11*), suggesting that PHb neurons are particularly susceptible to irregular changes in lighting conditions. T7 cycle exposure selectively affects the photo-responsiveness of PHb^{GABA} neurons. Therefore, we propose that under these irregular conditions, PHb^{GABA} neurons are recurrently receiving desynchronized signals from ipRGCs and thalamic networks, perturbing the mechanisms of integration of external and internal cues. Thus, the temporal inhibitory modulation of excitatory-relay PHb neurons is distorted, resulting in altered output signals and mood-related deficits (Fig. 6).

Together, these results described a retino-recipient inhibitory circuit within the thalamic PHb that processes daily changes in light to regulate thalamocortical circuits that control mood. Alterations in mood are common symptoms observed in a plethora of neuropsychiatric disorders, including major depression and seasonal affective disorder (*2*). Uncovering the cellular pathways by which light affects behavior would elucidate previously unidentified factors that contribute to mood dysregulation in neuropsychiatric disorders and may ultimately lead to innovative strategies to treat light-induced changes in mood and affective disorders.

MATERIALS AND METHODS

Animals

Adult mice (~3 months old) were housed at a temperature of 22°C with ad libitum access to food (standard chow) and water. WT mice of a mixed background (B6129SF1/J, stock number 101043), *GAD2*^{Cre} (stock number 019022), and *GAD2*^{mCherry} (stock number 023140) were obtained from the Jackson laboratory.

All animals were handled in accordance with guidelines from the Animal Care and Use Committees of the National Institute of Mental Health. All efforts were made to minimize animal pain and the number of animals used. When appropriate, experiments were randomized, and investigators were blinded to allocation during experiments and outcome assessment. Female and male mice were used for anatomical, electrophysiological, and RNA-seq studies. Only male mice were used for behavioral studies.

Activity measurements

Single-housed mice were exposed to regular light-dark cycles (T24, 12-hour light:12-hour dark) for 1 week to acclimate. Afterward, animals were housed either under the T24 cycle or irregular light cycles (T7 cycle) for 2 weeks. The ultradian T7 cycle consists of

3.5 hours of light followed by 3.5 hours of dark; light intensity is ~500 lux (provided by KOR 3500 K fluorescent bulbs), measured using a light meter (ExTech Lux Light Meter, 401025). Throughout the experiment, the general activity of mice was monitored using infrared motion detectors (IR) from Mini Mitter (Respironics) mounted to the top of the cages. Data were collected in 5-min bins using VitalView software (Mini Mitter, OR). The total activity and period lengths were calculated using ClockLab (Actimetrics, IL). Circadian period length was determined by fitting a regression line to the onsets of activity over a 10-day period using Clocklab (Actimetrics IL). Last, CT was calculated on the basis of individual animal locomotor activity, with CT12 defined as the onset of activity.

Stereotaxic injections

Mice were anesthetized with isoflurane, and AAVs or gΔRabies were stereotaxically delivered. Coordinates were determined following the Paxinos and Franklin mouse atlas (*40*). Coordinates for the PHb were −1.67 mm (from bregma), −3.23 mm (ventral), and ±0.67 mm (lateral). A 10-μl microcapillary pipette was pulled and loaded. Injections were performed using a microinjector (Nanojector III, Drummond Scientific Company). A heating pad was used to maintain animal body temperature during the surgery. Before surgery, systemic analgesics (meloxicam 0.1 mg/kg; Boehringer Ingelheim) were administered. A local analgesic was administered at the site of incision (lidocaine, 2 mg/kg; Fresenius Kabi). For anatomical analysis, mice were intracardially perfused with 4% paraformaldehyde at different times after injection (4 weeks after AAV injections or 5 days after gΔRabies injection), and the brains were subsequently sectioned on a cryostat. For experiments using gΔRabies virus, retinas were also dissected after perfusion and postfixed for 2 hours. Animals with starter cells (GFP^+ tdT^+) located exclusively in the PHb were studied; when starter cells were also observed in non-PHb areas, mice were excluded from the analysis.

The following viruses were used:

- AAV2/9-phSyn1(S)-Flex-tdTomato-t2a-SypEGFP-WPRE (Boston Children's Hospital Viral Core)
- AAV5-EF1a-DIO-hChR2(H134R)-EYFP-WPRE-pA (UNC vector core)
- retroAAV-EF1a Nuc-flox(mCherry)-EGFP (Addgene, #112677)
- AAV8/hSyn-FLEX-TVA-P2A-GFP-2A-oG (Salk Viral Core, #85225)
- EnvA G-Deleted Rabies-mCherry (Salk Viral Core, #32636)
- pAAV5-hSyn-DIO-hM3D(Gq)-mCherry (Addgene, #44361)
- AAV5-hSyn-DIO-mCherry (UNC vector core)
- AAV2-CAG-ChR2-GFP (UNC vector core)

Retinal injections

Retinal brain projections were visualized using intravitreal injections (1 μl) of the tracer cholera toxin β subunit (CTβ) fluorescently conjugated (Alexa Fluorophores, Thermo Fisher Scientific). Mice were anesthetized with isoflurane and placed under a stereo-microscope. A local analgesic was administered (lidocaine, 2 mg/kg; Fresenius Kabi). A glass needle (pulled 10-μl microcapillary tube, Sigma-Aldrich P0674) and a 10-μl Hamilton syringe were used to drive the solution into the vitreous chamber of the eye to ensure delivery specifically to the retina. Mice recovered from injections on a heating pad until they woke from anesthesia. After injections, animals were given a recovery period of 3 to 4 days. Mice were intracardially perfused with 4% paraformaldehyde, and brain samples were collected. Brains were postfixed overnight in the same fixative, and brain sections were obtained using the cryostat.

Histology/anatomical studies

For all studies, samples were collected at CT14, 2 hours after the onset of activity, unless otherwise noted.

Immunofluorescence

Brain sections and retinas were incubated in 0.1 M phosphate-buffered saline (PBS) with 3% goat or donkey serum (Vector Laboratories) and 0.3% Triton X-100 (Thermo Fisher Scientific) for 2 hours, and then incubated using the following antibodies for 1 to 2 days at 4°C: rabbit α-GABA (Sigma-Aldrich A-2052; 1:500), chicken α-GFP (AbCam Ab13970; 1:2000), rabbit α-c-Fos (Cell Signaling 2250S; 1:2500), rabbit α-Opn4 (Advanced Targeting Systems AB-N38; 1:1000), mouse immunoglobulin G1 α-SMI32 (BioLegend 801701; 1:200), goat α-tdTomato (LS-C340696; 1:1000), goat α-nNOS (Abcam ab1376; 1:300), rabbit α-VIP (ImmunoStar 20077; 1:1000), and rabbit α-NPY (Peninsula laboratory T-4070; 1:500). After the washing steps, Alexa-conjugated secondary antibodies were used (Invitrogen; 1:1000) for 2 hours at room temperature. Last, slides were mounted using Flouromount-G, with DAPI (4′,6-diamidino-2-phenylindole) (Invitrogen). Images were acquired using an ECLIPSE Ti2 inverted microscope (Nikon).

Light-mediated c-Fos induction

Mice were housed under either the T24 or T7 cycles for 2 weeks. They were then kept in darkness for 1 day to avoid any acute effects of light exposure. Two hours after the onset of activity (CT14, measured based on locomotor activity), mice were subjected to a 15-min light pulse (1000 lux) using 23-W compact fluorescent light bulbs (GE Daylight FLE10HT3/2/D). Mice were then kept in darkness for 90 min and, lastly, perfused transcardially with 4% paraformaldehyde.

Imaris

Images were opened on Imaris 9.2.1, and three-dimensional images were rendered, and then independent surfaces were created over the tdTomato and Syn-GFP signals. Surface grain size for tdTomato was 0.01 μm, and the threshold was adjusted to cover the staining and allow visualization of fine neuronal processes.

RNAscope in situ hybridization

Tools, slides, and equipment were cleaned with 70% ethanol and ribonuclease inhibitors (Fisher Scientific). Mice were euthanized by cervical dislocation, and brains were rapidly dissected and flash frozen with 2-methylbutane chilled on dry ice for 20 s. Subsequently, brains were stored at −80°C until sectioning. Brains were sliced using a cryostat (Leica), and sections (16 μm) were mounted on microscope slides. Slides containing sections were stored at −80°C until in situ hybridization processing. RNAscope procedures were conducted according to the Advanced Cell Diagnostics user manual. Slides were fixed with 10% neutral buffered formalin or 4% paraformaldehyde for 20 min at 4°C. Slides were subsequently washed twice for 1 min with PBS, before dehydration with 50% ethanol (1 × 5 min), 70% ethanol (1 × 5 min), and 100% ethanol (2 × 5 min). Slides were incubated in 100% ethanol at −20°C overnight. The next day, slides were dried at room temperature for 10 min. A hydrophobic pen was used to draw a hydrophobic barrier around the sections and allowed to dry for 10 to 15 min. Sections were then incubated with Protease Pretreat-4 solution for 20 min at room temperature.

Slides were washed with ddH_2O (2 × 1 min), before being incubated with the appropriate probes for 2 hours at 40°C in the HybEZ oven (Advanced Cell Diagnostics). Probes used were purchased from Advanced Cell Diagnostics as follows: *Slc32a1* (319191-C3), *Slc17a6* (319171-C2), *Gad1* (200951), *Gad2* (439371-C2), *Gabra5* (319481-C3), *Grin2a* (481831), *Camk2a* (445231-C3), *Gabra2* (435011), *Pvalb* (421931), and *Sst* (404631).

Chronic control of PHb^{GABA} function

$GAD2^{Cre}$ mice were stereotaxically injected with a *Cre*-dependent AAV5/DIO-hM3D-mCherry (Addgene) or AAV5/DIO-mCherry (Addgene) in the PHb region (bilateral injections). Mice recovered for 4 weeks with regular food and water under a T24 light-dark cycle. After 4 weeks, mice were given access to CNO dissolved in their drinking water. To achieve chronic activation, water + CNO was given to mice for 14 days, with fresh solution replaced daily (8 ml per day). The consumption of water + CNO was measured daily to ensure adequate drinking behavior and CNO treatment. Single-housed mice were held under T24 cycle during CNO treatment. After 2 weeks, behavioral tests were performed. The general activity of mice was monitored using IR sensors, and behavioral tests were performed during the active phase, between CT12 and CT14.

Behavioral tests

All behavioral tests were run in the Rodent Behavior Core at the National Institute of Mental Health.

Forced swim test

Forced swim test procedures were performed as previously described (*11*). Briefly, mice were placed in an inescapable container of water for 6 min. Behavioral responses were monitored using a video camera positioned in front of the apparatus and scored blindly by two experimenters. Time spent immobile for the last 4 min of the test was calculated and used for analysis.

Tail suspension test

Mice were suspended by the tail using tape. Two animals were tested simultaneously, with a white chamber preventing interaction between them. Mouse activity was recorded while suspended for 6 min. At the end of the session, mice were placed back in their home cage. Immobility time was scored blindly by two experimenters according to criteria previously described (*41*).

Novelty-suppressed feeding test

Mice were food deprived for 24 hours before the start of the test. The test was performed in a novel environment, which was an open field (60 cm by 60 cm square with black walls) with bright lighting (~500 lux). A food pellet was fixed to a small platform and placed in the center of the arena (*42*). The test began when a mouse was placed in the corner closest to the position of the experimenter. The latency for the mouse to eat the pellet, defined as when the animal sat on its haunches and took a bite, was recorded. Tests ran for 10 min. After the test, mice were transferred back to their home cage, and the amount of food consumed in 5 min was measured. The test was captured with an overhead mounted camera, and the video files were used to track the positions of the mouse using the Ethovision XT software (Noldus).

RNA isolation and sequencing

Mice housed under the T24 or T7 cycles were kept in darkness for 1 day before dissection to negate any acute effects of light. Brains were isolated and placed ventral side up on an ice-cold coronal slice brain matrix (Kent Scientific). A 1-mm coronal slice of the brain was sectioned using ice-cold razor blades positioned caudal to the optic chiasm. PHb tissue was collected, immediately placed in ice-cold Qiazol lysis reagent (Qiagen), and stored at −80 C. Bilateral PHb tissue samples were pooled from four mice per replicate with a total of four replicates per condition. RNA isolation was performed with the Qiagen RNEasy Lipid Tissue Mini kit following the manufacturer's instructions. cDNA was prepared from total RNA using the Ovation RNA-Seq System V2 (Tecan) and end repaired using the NEBNext End Repair Module (New England Biolabs). RNA-seq libraries were prepared from end-repaired cDNA with the TruSeq Stranded RNA Kit (Illumina). Libraries were pooled in an equimolar ratio before sequencing on an Illumina NovaSeq 6000 to a minimum depth of 128 million 150–base pair paired-end reads per library.

Bioinformatic analyses

The RNA-seq reads were mapped to the mouse genome (mm10) using STAR aligner (v2.4.2a). Differential gene expression analyses based on the negative binomial distribution and Wald significance tests were performed using the R package DESeq2 (version 1.28.1) and visualized as volcano plots. Standard multiple test correction was implemented using the Benjamini-Hochberg method for controlling the false discovery rate (FDR) of differentially expressed genes. Additional analyses and visualization used normalized count data that were extracted by first summing expression data per condition using the DESeq2 package function "*collapseReplicates*," and then performing a $\log_2$ variance stabilizing transformation (VST) from the fitted dispersion-mean relations using package function "*varianceStabilizingTransformation*." To infer functional relevance of differentially up-regulated genes, we performed gene ontology analysis on VST normalized counts using the Database for Annotation, Visualization, and Integrated Discovery.

We used GSEA to gain biological insight into the gene expression database, as previously reported (*27*). Normalized RNA-seq counts from different experimental groups were interrogated using a priori defined set of genes that are available in the Molecular Signatures Database v.7.4 (database: C5.go.bp.v7.4) (*43*). Statistically significant gene set enrichment cutoff was <0.05.

Quantitative PCR

PHb tissue samples were (bilaterally) dissected and immediately snap frozen in DNA loBind 1.5-ml tubes (Eppendorf, catalog no. 022431021) and then stored at −80°C. RNA isolation was performed using the RNeasy Micro kit (Qiagen, catalog no. 74004) with in-column DNase (deoxyribonuclease) treatment according to the instructions of the manufacturer. After electric motor tissue homogenization, PHb samples were pooled (n = 2 mice per pool) in the RNeasy MinElute spin column, resulting in a total of three pooled biological replicates for AAV/DREADD and AAV/control-injected samples. Isolated RNA was assessed for quality and concentration via RNA Tape Station. cDNA was subsequently prepared using a total of 200 ng of RNA per sample by following the manufacturer's instructions for SuperScript IV VILO (Thermo Fisher Scientific, catalog no. 11756050). qPCR reaction chemistry and thermocycle program were followed according to the manufacturer's instruction for TaqMan Fast Advanced Master Mix (Thermo Fisher Scientific, catalog no. 4444556). All qPCRs were run in duplicate on a QuantStudio 3 platform (Applied Biosystems, Design & Analysis Software version 1.4.3) using mouse-specific TaqMan primers. Last, relative gene expression was determined using the comparative C(T) method ($2^{-\Delta\Delta ct}$).

Whole-cell electrophysiology

For all studies, samples were collected between CT14 and CT16 (2 to 4 hours after the onset of activity). Mice were anesthetized and subsequently decapitated. Brains were removed rapidly and placed in ice-cold NMDG-based cutting solution containing 92 mM NMDG, 20 mM Hepes, 25 mM glucose, 30 mM $NaHCO_3$, 2.5 mM KCl, 1.2 mM $NaPO_4$ saturated with 95% O_2/5% CO_2 with an osmolarity of 303 to 306 mOsm (Wescorp). The brain was rapidly glued to a platform containing ice-cold NMDG-based cutting solution within a Leica VT1200 Vibratome. Coronal slices, 250 μm thick, containing the PHb were cut at a speed of 0.07 mm/s. Following slicing, sections were incubated in a chamber containing NMDG-based cutting solution for 5 to 10 min at 34°C. Slices were subsequently transferred to a chamber filled with modified holding artificial cerebrospinal fluid (aCSF) saturated with 95% O_2/5% CO_2 containing 92 mM NaCl, 20 mM Hepes, 25 mM glucose, 30 mM $NaHCO_3$, 2.5 mM KCl, 1.2 mM $NaPO_4$ (303 to 306 mOsm) at room temperature for at least 1 hour. Slices remained in this solution until being transferred to the recording chamber.

Whole-cell patch clamp electrophysiology studies were performed as previously described (*44*, *45*). For recordings, the recording chamber was perfused with a pump (World Precision Instruments) at a flow rate of 1.5 to 2.0 ml per minute with aCSF containing 126 mM NaCl, 2.5 mM KCl, 1.4 mM NaH_2PO_4, 1.2 mM $MgCl_2$, 2.4 $CaCl_2$, 25 mM $NaHCO_3$, and 11 mM glucose (303 to 305 mOsm). Cells were visualized using IR–differential interference contrast optics on an inverted Olympus BX5iWI microscope. Neurons were voltage clamped using a Multiclamp 700B amplifier (Molecular Devices). Data were filtered at 2 kHz and digitized at 20 kHz using a 1440A Digidata Digitizer (Molecular Devices). Series resistance (10 to 20 megohms) was monitored using a −5-mV voltage step. Cells with >20% change in series resistance were discarded from further analysis.

For biophysical isolation of GABA-A receptor–mediated optogenetic-evoked IPSCs (oIPSCs), we used glass microelectrodes (3 to 5 megohms) containing 117 mM cesium methanesulfonate, 20 mM Hepes, 0.4 mM EGTA, 2.8 mM NaCl, 5 mM TEA-Cl, 4 mM Mg–adenosine triphosphate (ATP), 0.4 Na–guanosine triphosphate (GTP), and 5 QX-314 (280 to 285 mOsm). sIPSCs and mIPSCs were recorded at 0 mV in the presence of DNQX (10 μM) and AP-5 (50 μM) to block fast excitatory transmission. $GAD2^{Cre}$ mice were injected with an AAV5-EF1a-DIO-ChR2-eYFP into the PHb (60 nl). oIPSCs were evoked using a PE-300 Cool LED (1-ms pulse duration; 3 to 60 mW) at a holding potential of 0 mV. To establish that oIPSCs from PHb^{GABA} neurons were from bona fide monosynaptic connections onto PHb relay neurons, we first washed in TTX (1 μM; Tocris) for 5 min, and then TTX and 4-aminopyridine (50 μM; Sigma-Aldrich). For comparison of PHb^{GABA} oIPSCs between control and T7 animals, stable oIPSCs were first established using 30-mW stimulation intensity and recorded for approximately 5 min. Subsequently, oIPSC input-output curves were generated by incrementally increasing stimulation intensity. Trains of stimulation (10 pulses; 2, 5, 10, and 20 Hz) were applied every 30 s to determine paired pulse ratios and short-term plasticity. The order of train stimulation frequencies was counterbalanced between cells. After recordings, images of recording location and eYFP fluorescence were acquired. For a subset of experiments, slices were fixed with 4% paraformaldehyde for quantification of eYFP fluorescence between T24 and T7 cycle-housed mice.

For whole-cell recordings of intrinsic excitability, we used glass microelectrodes (3 to 5 megohms) containing 135 mM K-gluconate, 10 mM Hepes, 4 mM KCl, 4 mM Mg-ATP, and 0.3 mM Na-GTP, and, in some cases, 0.1% Biocytin. Biocytin (1 to 1.5%; Sigma-Aldrich) was added to a K-gluconate–based internal solution on the day of the recording. For intrinsic excitability, after membrane rupture in voltage clamp, cells were switched to the current clamp configuration without holding current injection.

Quantification and statistical analysis

Calculation of sample size per experiment was determined, or confirmed by post hoc analyses, using G*Power 3 software, as previously described (*46*, *47*). Rostral, middle, and caudal PHb regions were determined on the basis of the pattern of retinal innervation and coronal brain coordinates (~distance to bregma) obtained from the Paxinos and Franklin mouse atlas (*40*): rostral PHb = −1.42 to 1.62 mm; middle PHb = −1.66 to −1.86 mm; caudal PHb = −1.90 to −2.10 mm.

Statistical analysis of results was performed using Student's *t* test [parametric or nonparametric (Mann–Whitney)] or analysis of variance followed by Tukey's or Sidak's multiple comparisons tests, as stated. All the analyses were done using GraphPad Prism, version 7.0a. Each figure legend contains statistical reports for each comparison.

SUPPLEMENTARY MATERIALS

Supplementary material for this article is available at https://science.org/doi/10.1126/sciadv.abn3567

View/request a protocol for this paper from *Bio-protocol*.

REFERENCES AND NOTES

1. T. Alterman, S. E. Luckhaupt, J. M. Dahlhamer, B. W. Ward, G. M. Calvert, Prevalence rates of work organization characteristics among workers in the U.S.: Data from the 2010 National Health Interview Survey. *Am. J. Ind. Med.* **56**, 647–659 (2013).
2. S. J. Russo, E. J. Nestler, The brain reward circuitry in mood disorders. *Nat. Rev. Neurosci.* **14**, 609–625 (2013).
3. E. C. Marqueze, S. Vasconcelos, J. Garefelt, D. J. Skene, C. R. Moreno, A. Lowden, Natural light exposure, sleep and depression among day workers and shiftworkers at Arctic and equatorial latitudes. *PLOS ONE* **10**, e0122078 (2015).
4. S. Hattar, H. W. Liao, M. Takao, D. M. Berson, K. W. Yau, Melanopsin-containing retinal ganglion cells: Architecture, projections, and intrinsic photosensitivity. *Science* **295**, 1065–1070 (2002).
5. D. M. Berson, F. A. Dunn, M. Takao, Phototransduction by retinal ganglion cells that set the circadian clock. *Science* **295**, 1070–1073 (2002).
6. T. M. Schmidt, S.-K. Chen, S. Hattar, Intrinsically photosensitive retinal ganglion cells: Many subtypes, diverse functions. *Trends Neurosci.* **34**, 572–580 (2011).
7. T. A. LeGates, C. M. Altimus, H. Wang, H.-K. Lee, S. Yang, H. Zhao, A. Kirkwood, E. T. Weber, S. Hattar, Aberrant light directly impairs mood and learning through melanopsin-expressing neurons. *Nature* **491**, 594–598 (2012).
8. D. G. Aytürk, A. M. Castrucci, D. E. Carr, S. R. Keller, I. Provencio, Lack of melanopsin is associated with extreme weight loss in mice upon dietary challenge. *PLOS ONE* **10**, e0127031 (2015).
9. M. Tatsumoto, M. Yamakawa, K. Okajima, K. Hirata, Contribution of intrinsically photosensitive retinal ganglion cells in the photophobia of migraine patients. *J. Neurol. Sci.* **357**, e168–e169 (2015).
10. R. Feng, L. Li, H. Yu, M. Liu, W. Zhao, Melanopsin retinal ganglion cell loss and circadian dysfunction in Alzheimer's disease (review). *Mol. Med. Rep.* **13**, 3397–3400 (2016).
11. D. C. Fernandez, P. M. Fogerson, L. Lazzerini Ospri, M. B. Thomsen, R. M. Layne, D. Severin, J. Zhan, J. H. Singer, A. Kirkwood, H. Zhao, D. M. Berson, S. Hattar, Light affects mood and learning through distinct retina-brain pathways. *Cell* **175**, 71–84.e18 (2018).
12. K. An, H. Zhao, Y. Miao, Q. Xu, Y.-F. Li, Y.-Q. Ma, Y.-M. Shi, J.-W. Shen, J.-J. Meng, Y.-G. Yao, Z. Zhang, J.-T. Chen, J. Bao, M. Zhang, T. Xue, A circadian rhythm-gated subcortical pathway for nighttime-light-induced depressive-like behaviors in mice. *Nat. Neurosci.* **23**, 869–880 (2020).
13. S. M. Sherman, R. W. Guillery, The role of the thalamus in the flow of information to the cortex. *Philos. Trans. R. Soc. B Biol. Sci.* **357**, 1695–1708 (2002).

14. D. H. Hubel, T. N. Wiesel, Receptive fields, binocular interaction and functional architecture in the cat's visual cortex. *J. Physiol.* **160**, 106–154 (1962).
15. E. G. Jones, in *The Thalamus* (Springer US, 1985), pp. 85–149.
16. M. M. Halassa, S. M. Sherman, Thalamocortical circuit motifs: A general framework. *Neuron* **103**, 762–770 (2019).
17. S. M. Sherman, Interneurons and triadic circuitry of the thalamus. *Trends Neurosci.* **27**, 670–675 (2004).
18. M. M. Halassa, L. Acsády, Thalamic inhibition: Diverse sources, diverse scales. *Trends Neurosci.* **39**, 680–693 (2016).
19. T. A. LeGates, D. C. Fernandez, S. Hattar, Light as a central modulator of circadian rhythms, sleep and affect. *Nat. Rev. Neurosci.* **15**, 443–454 (2014).
20. R. Noseda, V. Kainz, M. Jakubowski, J. J. Gooley, C. B. Saper, K. Digre, R. Burstein, A neural mechanism for exacerbation of headache by light. *Nat. Neurosci.* **13**, 239–245 (2010).
21. J. L. Morgan, J. W. Lichtman, An individual interneuron participates in many kinds of inhibition and innervates much of the mouse visual thalamus. *Neuron* **106**, 468–481.e2 (2020).
22. S. El Mestikawy, Å. Wallén-Mackenzie, G. M. Fortin, L. Descarries, L. E. Trudeau, From glutamate co-release to vesicular synergy: Vesicular glutamate transporters. *Nat. Rev. Neurosci.* **12**, 204–216 (2011).
23. Y. Li, V. G. Lopez-Huerta, X. Adiconis, K. Levandowski, S. Choi, S. K. Simmons, M. A. Arias-Garcia, B. Guo, A. Y. Yao, T. R. Blosser, R. D. Wimmer, T. Aida, A. Atamian, T. Naik, X. Sun, D. Bi, D. Malhotra, C. C. Hession, R. Shema, M. Gomes, T. Li, E. Hwang, A. Krol, M. Kowalczyk, J. Peça, G. Pan, M. M. Halassa, J. Z. Levin, Z. Fu, G. Feng, Distinct subnetworks of the thalamic reticular nucleus. *Nature* **583**, 819–824 (2020).
24. R. I. Martinez-Garcia, B. Voelcker, J. B. Zaltsman, S. L. Patrick, T. R. Stevens, B. W. Connors, S. J. Cruikshank, Two dynamically distinct circuits drive inhibition in the sensory thalamus. *Nature* **583**, 813–818 (2020).
25. P. Jager, G. Moore, P. Calpin, X. Durmishi, I. Salgarella, L. Menage, Y. Kita, Y. Wang, D. W. Kim, S. Blackshaw, S. R. Schultz, S. Brickley, T. Shimogori, A. Delogu, Dual midbrain and forebrain origins of thalamic inhibitory interneurons. *eLife* **10**, e59272 (2021).
26. M. Evangelio, M. García-Amado, F. Clascá, Thalamocortical projection neuron and interneuron numbers in the visual thalamic nuclei of the adult C57BL/6 mouse. *Front. Neuroanat.* **12**, 27 (2018).
27. A. Subramanian, P. Tamayo, V. K. Mootha, S. Mukherjee, B. L. Ebert, M. A. Gillette, A. Paulovich, S. L. Pomeroy, T. R. Golub, E. S. Lander, J. P. Mesirov, Gene set enrichment analysis: A knowledge-based approach for interpreting genome-wide expression profiles. *Proc. Natl. Acad. Sci.* **102**, 15545–15550 (2005).
28. B. L. Roth, DREADDs for neuroscientists. *Neuron* **89**, 683–694 (2016).
29. C. Bainier, M. Mateo, M.-P. Felder-Schmittbuhl, J. Mendoza, Circadian rhythms of hedonic drinking behavior in mice. *Neuroscience* **349**, 229–238 (2017).
30. G. R. Penny, M. Conley, D. E. Schmechel, I. T. Diamond, The distribution of glutamic acid decarboxylase immunoreactivity in the diencephalon of the opossum and rabbit. *J. Comp. Neurol.* **228**, 38–56 (1984).
31. P. Arcelli, C. Frassoni, M. C. Regondi, S. De Biasi, R. Spreafico, GABAergic neurons in mammalian thalamus: A marker of thalamic complexity? *Brain Res. Bull.* **42**, 27–37 (1997).
32. O. P. Ottersen, J. Storm-Mathisen, GABA-containing neurons in the thalamus and pretectum of the rodent. An immunocytochemical study. *Anat. Embryol. (Berl).* **170**, 197–207 (1984).
33. M. Leist, M. Datunashvilli, T. Kanyshkova, M. Zobeiri, A. Aissaoui, M. Cerina, M. N. Romanelli, H. C. Pape, T. Budde, Two types of interneurons in the mouse lateral geniculate nucleus are characterized by different h-current density. *Sci. Reports* **6**, 24904 (2016).
34. A. Kepecs, G. Fishell, Interneuron cell types are fit to function. *Nature* **505**, 318–326 (2014).
35. D. Plenz, J. R. Wickens, The striatal skeleton: Medium spiny projection neurons and their lateral connections. *Handb. Behav. Neurosci.* **24**, 121–136 (2016).
36. M. Hashimoto, A. Yamanaka, S. Kato, M. Tanifuji, K. Kobayashi, H. Yaginuma, Anatomical evidence for a direct projection from Purkinje cells in the mouse cerebellar vermis to medial parabrachial nucleus. *Front. Neural Circuits* **12**, 6 (2018).
37. K. Toth, Z. Borhegyi, T. Freund, Postsynaptic targets of GABAergic hippocampal neurons in the medial septum-diagonal band of broca complex. *J. Neurosci.* **13**, 3712–3724 (1993).
38. L. Seress, C. Ribak, GABAergic cells in the dentate gyrus appear to be local circuit and projection neurons. *Exp. Brain Res.* **50**, 173–182 (1983).
39. S. Jinno, Structural organization of long-range GABAergic projection system of the hippocampus. *Front. Neuroanat.* **0**, 13 (2009).
40. K. B. J. Franklin, G. Paxinos, *Paxinos and Franklin's the Mouse Brain in Stereotaxic Coordinates* (Academic Press, 2019).
41. A. Can, D. T. Dao, C. E. Terrillion, S. C. Piantadosi, S. Bhat, T. D. Gould, The tail suspension test. *J. Vis. Exp.* , e3769 (2012).
42. B. A. Samuels, R. Hen, Novelty-suppressed feeding in the mouse. *NeuroMethods* **63**, 107–121 (2011).
43. A. Liberzon, C. Birger, H. Thorvaldsdóttir, M. Ghandi, J. P. Mesirov, P. Tamayo, The molecular signatures database (MSigDB) hallmark gene set collection. *Cell Syst.* **1**, 417–425 (2015).
44. H. A. Tejeda, J. Wu, A. R. Kornspun, M. Pignatelli, V. Kashtelyan, M. J. Krashes, B. B. Lowell, W. A. Carlezon, A. Bonci, Pathway- and cell-specific kappa-opioid receptor modulation of excitation-inhibition balance differentially gates D1 and D2 accumbens neuron activity. *Neuron* **93**, 147–163 (2017).
45. M. Pignatelli, H. A. Tejeda, D. J. Barker, L. Bontempi, J. Wu, A. Lopez, S. Palma Ribeiro, F. Lucantonio, E. M. Parise, A. Torres-Berrio, Y. Alvarez-Bagnarol, R. A. M. Marino, Z. L. Cai, M. Xue, M. Morales, C. A. Tamminga, E. J. Nestler, A. Bonci, Cooperative synaptic and intrinsic plasticity in a disynaptic limbic circuit drive stress-induced anhedonia and passive coping in mice. *Mol. Psychiatry* **26**, 1860–1879 (2021).
46. F. Faul, E. Erdfelder, A.-G. Lang, A. Buchner, G*Power 3: A flexible statistical power analysis program for the social, behavioral, and biomedical sciences. *Behav. Res. Methods* **39**, 175–191 (2007).
47. J. Charan, N. Kantharia, How to calculate sample size in animal studies? *J. Pharmacol. Pharmacother.* **4**, 303–306 (2013).

Acknowledgments: We would like to thank all the members of the Section on Light and Circadian Rhythms (SLCR) at the National Institute of Mental Health (NIMH) for support and discussion. In addition, we thank the NIH Intramural Sequencing Center (NISC) for help with the library preparation and sequencing and the NIMH IRP Rodent Behavioral Core for support with mouse behavioral tasks. **Funding:** This work was supported by the Intramural Research Program (IRP) at the NIMH (ZIAMH002964). **Author contributions:** Conceptualization: D.C.F., S.H., and H.T. Methodology: T.W., K.M.D., H.Y.C., M.B.T., H.W., M.E.M., H.T., and D.C.F. Writing—original draft: D.C.F. Writing—review and editing: T.W., K.M.D., H.Y.C., M.B.T., M.E.M., S.H., and H.T. Funding acquisition: S.H. and H.T. **Competing interests:** The authors declare that they have no competing interests. **Data and materials availability:** All data needed to evaluate the conclusions in the paper are present in the paper and/or the Supplementary Materials. The accession number for the raw and processed gene expression data from the RNA sequencing experiments reported in this paper is GEO: GSE199713 (link: www.ncbi.nlm.nih.gov/geo/query/acc.cgi?acc=GSE199713).

Submitted 29 November 2021
Accepted 27 April 2022
Published 10 June 2022
10.1126/sciadv.abn3567